

Observation of Electron Temperature Gradient Driven Low-Frequency Instabilities in Magnetized Plasma

Chanho MOON, Shuichi TAMURA, Toshiro KANEKO, and Rikizo HAKAKEYAMA

Department of Electronic Engineering, Tohoku University, Sendai 980-8579, Japan

(Received: 1 November 2009 / Accepted: 8 March 2010)

Perpendicular Electron temperature gradient (ETG) is formed in a magnetized plasma by superimposing low-temperature thermionic electrons emitted from a tungsten hot plate upon high-temperature electrons of an electron cyclotron resonance (ECR) plasma, which pass through two different-sized negatively-biased mesh grids. It is experimentally observed that low-frequency instabilities are driven by the ETG. Moreover, the characteristics of the ETG driven low-frequency instabilities are controlled by the plasma parameters such as radial potential and density profiles which are varied by the bias voltages of the hot plate and the power of a microwave for the ECR plasma.

Keywords: electron temperature gradient, low-frequency instabilities, thermionic electron, ECR plasma.

1. Introduction

In recent years, anomalous plasma heat transports in tokamaks are an outstanding issue, which are difficult to be explained clearly even though many researchers try to understand the mechanism of the heat transports in fusion devices [1-6]. There are strong experimental evidences that the anomalous heat transports are attributed to various kinds of small-scale instabilities driven by temperature gradients [7-12]. As is well known, there are two types of temperature gradient instabilities, namely ion temperature gradient (ITG mode) and electron temperature gradient (ETG mode) instabilities. It is reported that the ITG mode plays an important role in an ion channel heat transport and an ExB sheared flow can make the ITG mode stable [13-15]. On the other hand, the ETG mode is the plausible candidate for the anomalous electron heat transport of the tokamak devices and it is recognized to be difficult to stabilize the ETG mode by the $E \times B$ sheared flow because the ETG mode has a smaller spatial scale and a larger linear growth rate, and as a result, it is not strongly affected by the sheared flow. Actually, it is seen that the instability is driven by the ETG and nonlinear effects of the ETG modes generate the significant electron transport. Although there are some earlier theoretical [16,17], numerical [18,19], and experimental [20-23] studies on the ETG mode, the output is not enough to explain the problems clearly, which is caused by the restricted experimental condition in the magnetically confined fusion plasmas.

In the laboratory experiments, on the other hand, several advanced techniques have been applied to the control of the electron temperature [24,25], but it is difficult to realize the spatially different electron

temperature at a localized area. To solve this problem, we suggest generating the high and low temperature electrons separately and mixing them with spatial control. Thus the aim of this work is to control the ETG by using a thermionic electron superimposed electron cyclotron resonance (ECR) plasma and applying voltages to two different-sized mesh grids in a basic plasma device in order to investigate the effects of the ETG on low frequency fluctuations.

2. Experimental apparatus and method

Experiments are carried out in a linear machine (Q_T -Upgrade) of Tohoku University, which is shown in Fig. 1. In order to perform the experiment we divide the machine into two sections. One is called as a source region where the ECR plasma with high electron temperature is generated and the other is called as an

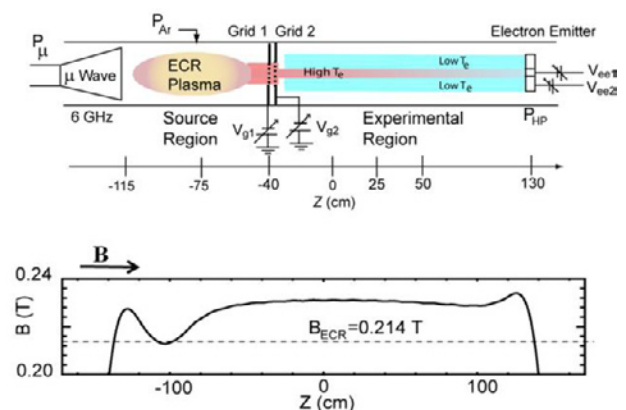


Fig. 1. Schematic diagram of an experimental apparatus with an axial profile of magnetic

experimental region where low-temperature thermionic electrons are superimposed on the high-temperature ECR plasma. Here, the axial center of the machine is defined as $z = 0$ cm. In the source region, a magnetic field is well shaped and the bottom of the well is set to be the electron cyclotron resonance field $B_{\text{ECR}} = 0.214$ T. Ar gas (pressure $P_{\text{Ar}} = 2.0 \times 10^{-4}$ Torr) and a microwave (frequency 6 GHz and power $P_{\mu} = 10 \sim 200$ W) are used to control the electron density and temperature in the experimental region. Two types of stainless mesh grids [grid 1 (ϕ 6 cm, 10 mesh/inch) and grid 2 (doughnut shape, OD: ϕ 6 cm, ID: ϕ 3 cm, 30 mesh/inch)] are located at $z \approx -40$ cm and divide the source region from the experimental region.

A tungsten (W) hot plate set in the end of the experimental region is heated by applying DC power $P_{\text{HP}} = 3$ kW and generates the low-temperature thermionic electrons ($T_e = 0.2$ eV), which works as an electron emitter. Since the electron emitter is concentrically segmented into three sections, a radial profile of the space potential is controllable by applying different bias voltages between central (V_{ee1}) and peripheral (V_{ee2}) sections of the electron emitter. Here, the outermost section is always grounded in this experiment. A Langmuir probe is used to measure the radial profiles of plasma parameters at $z = 0$ cm in the experimental region. Moreover, a two-dimensional Γ -shaped probe is used to measure a two-dimensional profile of the fluctuations. Figure 2 presents a schematic model of the ETG formation. The high-temperature electrons of the ECR plasma pass through the slightly negatively-biased grid 1, by which the density of the high-temperature electrons in the experimental region is

adjusted. Furthermore, since the microwave is prevented from passing through the grid 1, there is no additional electron heating in the experimental region. The negatively-biased grid 2 which has the doughnut shape of mesh prevents the electrons in the peripheral regions from penetrating into the experimental region. Therefore, the high temperature electrons only in the central region pass through the grid 2. On the other hand, the low-temperature electrons are generated by the W hot plate on the other side and superimposed on the high-temperature electrons of the ECR plasma. These large amounts of low temperature electrons can decrease the electron temperature especially in the peripheral region and compensate the density gradient of the ECR plasma penetrating the grid 2. Therefore, the large ETG is formed in the experimental region keeping the radial density profile uniform.

3. Results and Discussion

Figure 3 shows dependences of the electron temperature on the grid bias voltages (V_{g1} , V_{g2}). When the applied bias voltage of the grid 2 decreases to minus several volts, the electron temperature only in the peripheral region rapidly decreases, but the electron temperature in the central region is almost constant. Since

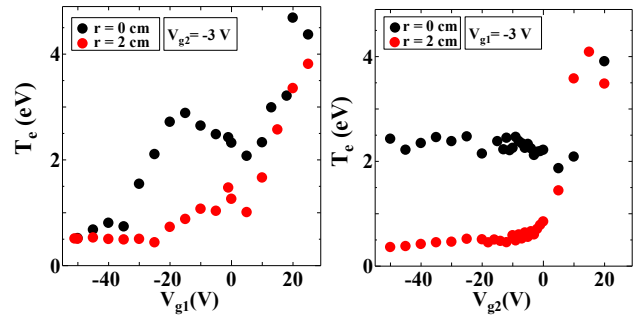


Fig. 3. Electron temperature (T_e) in the central and peripheral regions as a function of the grid bias voltages (V_{g1} , V_{g2}).

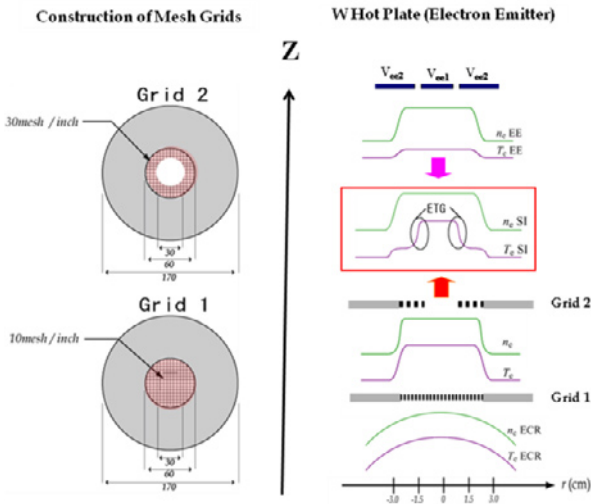


Fig. 2. Schematic model of ETG formation in the experimental region using the thermionic electron superimposed ECR plasma.

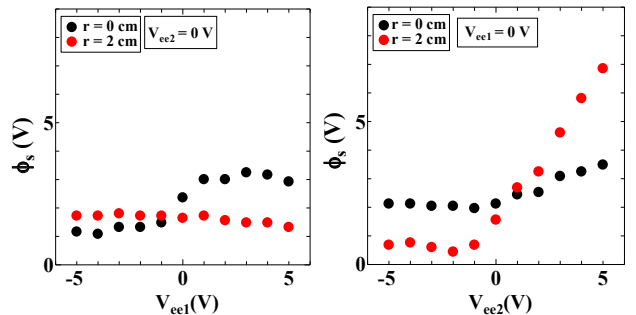


Fig. 4. Space potential (ϕ_s) in the central and peripheral regions as a function of the electron emitter bias voltages (V_{ee1} , V_{ee2}).

the electron temperature can be controlled by changing the bias voltages of V_{g1} and V_{g2} , it is possible to make the temperature gradient easily.

Figure 4 gives dependences of the space potential (ϕ_s) on the bias voltages of the electron emitter in the central (V_{ee1}) and peripheral (V_{ee2}) regions. In the case of changing V_{ee1} , the space potential only in the central region is changed definitely, but the space potential in the peripheral region is almost constant. In contrast, V_{ee2} can change the space potential only in the peripheral region, keeping the central space potential constant. Therefore, the radial profile of the space potential can be controlled by changing the biased voltage V_{ee1} and V_{ee2} .

Figure 5 presents typical radial profiles of electron temperature (T_e), density (n_e), and space potential (ϕ_s) when their gradients are controlled by the bias voltage of the mesh grids and the electron emitters. When $V_{g2} = -3$ V which corresponds to the floating potential of the grid 2 [Fig. 5(a)], the electron temperature has no significant difference at the boundary between the central and peripheral regions, which is indicated by dotted lines in the figure. On the other hand, when V_{g2} is deeply negatively biased ($= -30$ V), the electron temperature in the peripheral region drastically decreases, and as a result, the large ETG is formed at the boundary as shown in Fig. 5(b). The electron density has the sharp gradient at $r \simeq 1$

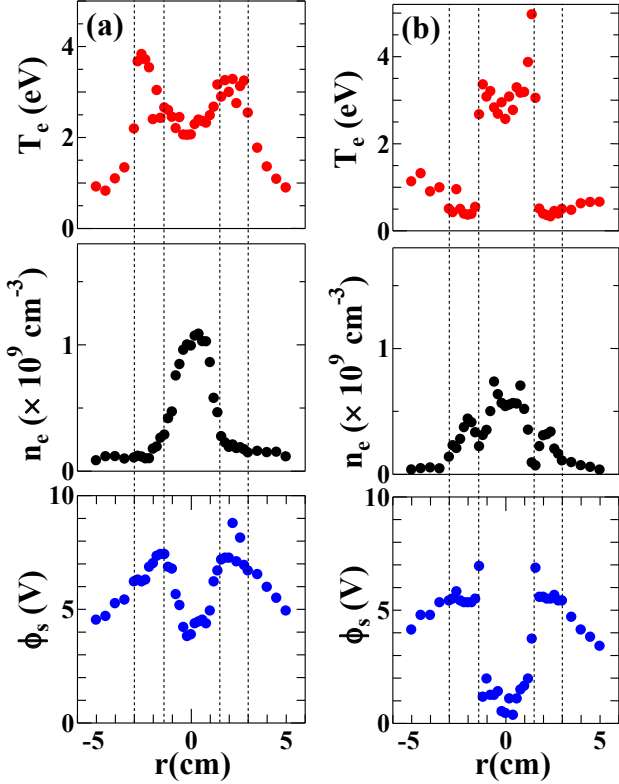


Fig. 5. Radial profiles of electron temperature, density, and space potential. $V_{ee1} = 0$ V, $V_{ee2} = +5$ V, $P_{\mu} = 70$ W. (a) $V_{g1} = V_{g2} = -3$ V, (b) $V_{g1} = -20$ V, $V_{g2} = -30$ V.

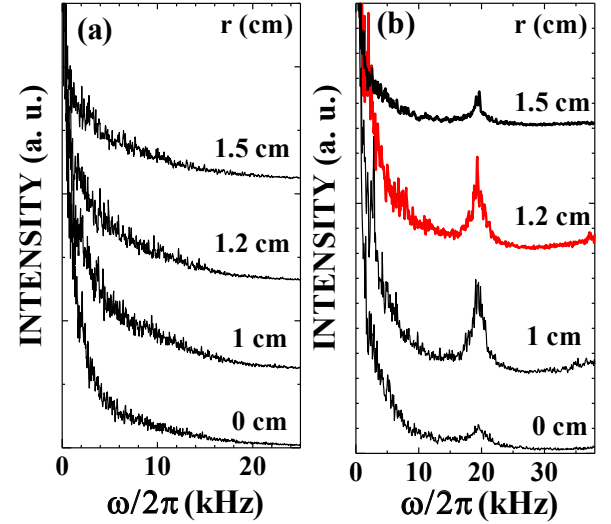


Fig. 6. Frequency spectra of electron saturation current I_{es} under the same conditions as in Fig. 5.

cm in Fig. 5(a), while has the relatively flat profile in Fig. 5(b). Here, since V_{ee1} is not equal to V_{ee2} , a radial potential gradient, i.e., radial electric field is generated at the boundary in both the cases.

Figure 6 shows frequency spectra of electron saturation current under the same conditions as in Fig. 5. In the case of Fig. 6(a), the fluctuation is not excited in the absence of the ETG even when the density gradient is generated at $r \simeq 1$ cm and the potential gradient is relatively large. On the other hand, it is found that low-frequency (20 kHz) fluctuations are driven in the case that the ETG exists, as seen in Fig. 6(b). Since the

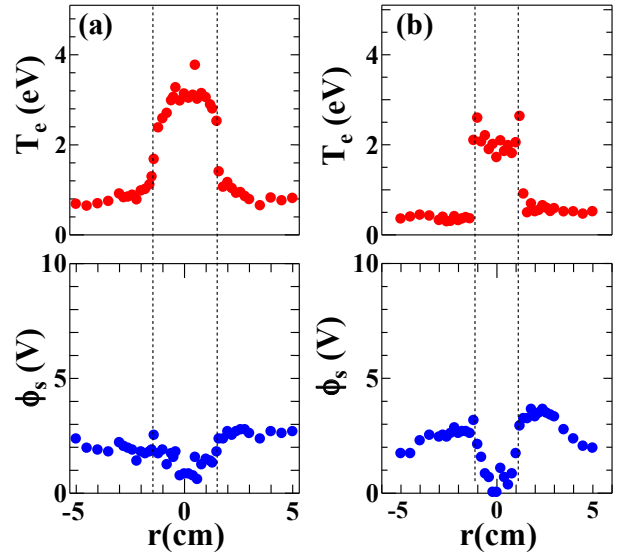


Fig. 7. Radial profiles of electron temperature and space potential. (a) $P_{\mu} = 200$ W, $V_{g1} = -10$ V, $V_{g2} = -30$ V, $V_{ee1} = V_{ee2} = 0$ V, (b) $P_{\mu} = 10$ W, $V_{g1} = -20$ V, $V_{g2} = -30$ V, $V_{ee1} = 0$ V, $V_{ee2} = +3$ V.

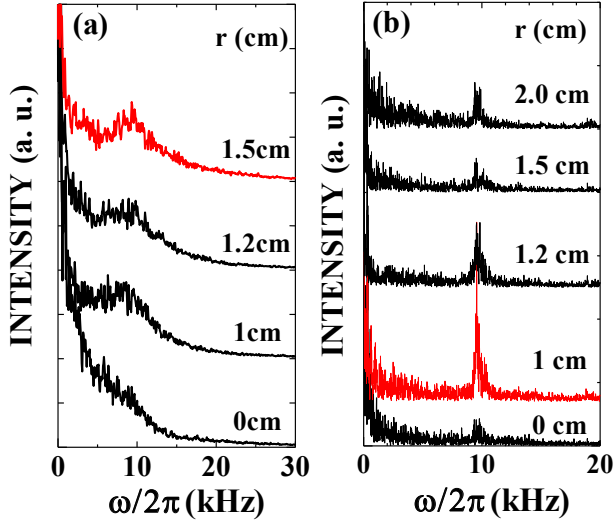


Fig. 8. Frequency spectra of electron saturation current \tilde{I}_{es} under the same conditions as in Fig. 7.

fluctuations are excited at $r = 1\text{--}1.5$ cm where the ETG has the maximum value, they are confirmed to be caused by the ETG. In this case, however, the steep space potential gradient coexists as already mentioned in Fig. 5. Therefore, these fluctuations seem to be related to not only the ETG, but also the potential gradient which generates an $E \times B$ flow and its shear.

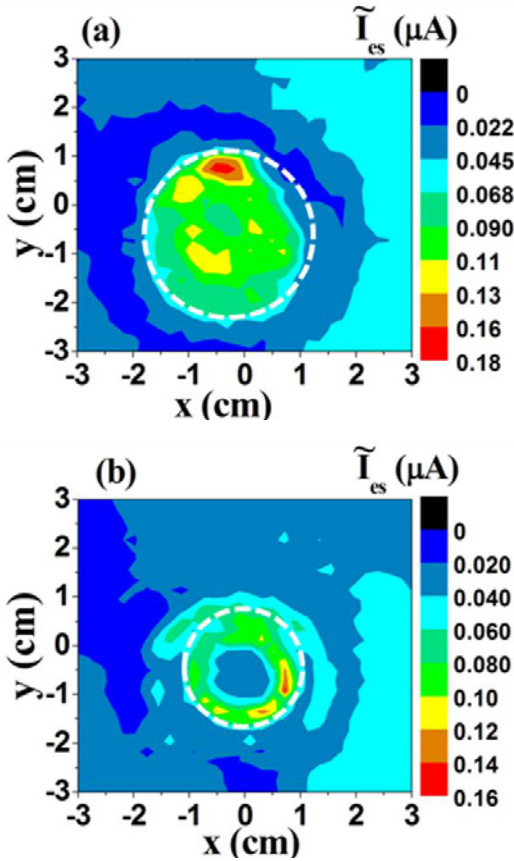


Fig. 9. 2-D profiles of fluctuation amplitude of electron saturation current \tilde{I}_{es} , $V_{g1} = -20\text{V}$, $V_{g2} = -30\text{V}$. (a) $P_{\mu} = 70\text{ W}$, $V_{ee1} = 0\text{ V}$, $V_{ee2} = +5\text{V}$, (b) $P_{\mu} = 10\text{ W}$, $V_{ee1} = 0\text{ V}$, $V_{ee2} = +3\text{V}$.

In order to clarify the effects of the $E \times B$ flow and its shear on the ETG driven fluctuations, we change the radial potential profile by means of the bias voltages of the electron emitter.

Two different radial potential profiles with ETG are realized as presented in Fig. 7. The radial profile of the space potential is almost flat for $V_{ee1} = V_{ee2} = 0\text{ V}$ [Fig. 7(a)], while the space potential has the large gradient in the case that V_{ee2} is changed to 3 V [Fig. 7(b)]. In addition, the temperature gradient regions are different between the cases of Figs. 7(a) and 7(b), which are controlled by the microwave power.

Figure 8 shows the frequency spectra under the same conditions as in Fig. 7. Since the fluctuation amplitude in Fig. 8(a) is smaller than that in Fig. 8(b), it is considered that the low-frequency fluctuation is driven by the ETG in cooperation with the $E \times B$ flow and its shear. Moreover, the radial position where the fluctuation amplitude has maximum value is $r = 1.5$ cm in the case of Fig. 8(a), while $r = 1$ cm in the case of Fig. 8(b). These radial positions correspond to the region of the ETG.

Figure 9 gives two-dimensional profiles of the fluctuation amplitude by using the two-dimensional

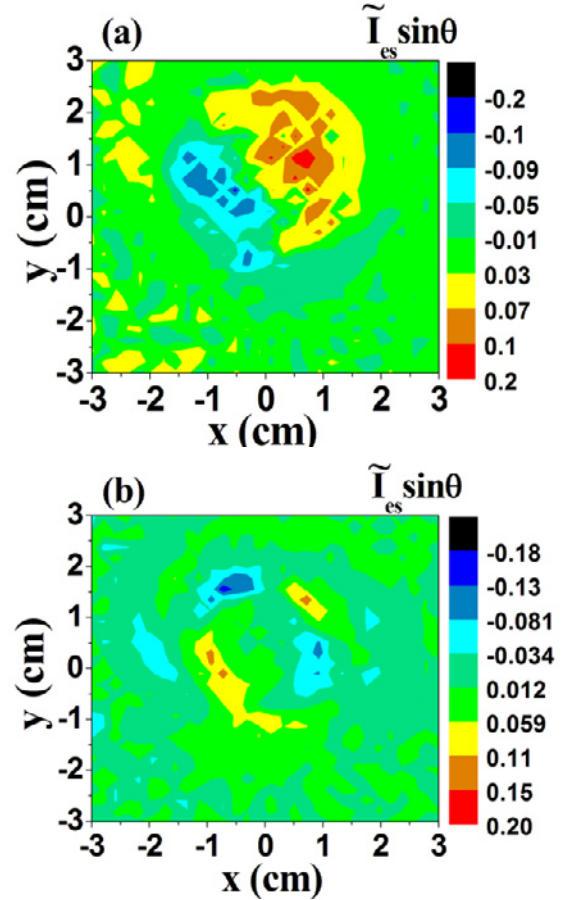


Fig. 10. 2-D profiles of fluctuation structure which is plotted as the product of fluctuation amplitude \tilde{I}_{es} and sin function of fluctuation phase θ .

Γ -shaped probe and the Langmuir probe as a reference probe. The experimental conditions of Figs. 9(a) and 9(b) correspond to those in Figs. 5(b) and 7(b), respectively. Both of the figures show doughnut shapes which indicate that the strong fluctuation grows in the region of the generated ETG, where the diameters of the white-dotted circles indicating the maximum fluctuation amplitude are different. In the case of the high microwave power, the diameter is larger than that in the case of the low microwave power depending on the region of the ETG.

The two-dimensional profiles of the fluctuation structure under the same condition as in Fig. 9 are presented in Fig. 10. The fluctuation structure is defined as the product of the fluctuation amplitude $\tilde{\gamma}_{es}$ and sin function of the fluctuation phase θ . It is found that they have different azimuthal mode numbers. In the case of Fig. 10(a), the azimuthal mode number is one, where the frequency is 20 kHz which is shown in Fig. 6(b). On the other hand, the azimuthal mode number in Fig. 10(b) is changed into two and the frequency is 10 kHz as shown in Fig. 8(b). The difference in the frequency is explained by the Doppler shift effect of the $E \times B$ rotation, because the radial electric field in Fig. 10(a), which is shown in Fig. 5(b), is much larger than that in Fig. 10(b), which is shown in Fig. 7(b).

The azimuthal mode number is considered to be determined by the region where the ETG exists, however, the detailed mechanism is under investigation.

4. Summary

We have developed a novel method to form and control the electron temperature gradient (ETG) in the magnetized plasma by using the thermionic electron superimposed electron cyclotron resonance plasma. It is found that the ETG can be controlled by means of the two grids and the power of the microwave, which can modify the density of high temperature electrons in the experimental region. In addition, the low frequency fluctuations are observed in the region where the ETG has the maximum value and the radial electric field exists. Therefore, the fluctuation is considered to be excited by the coexistence of the ETG, the $E \times B$ flow, and its shear.

Acknowledgements

The authors are indebted to H. Ishida for his technical assistance. The work was supported by a Grant-in-Aid for Scientific Research from the Ministry of Education, Culture, Sports, Science and Technology, Japan.

References

- [1] F. Jenko, W. Dorland, and G. W. Hammett, *Phys. Plasmas* **8**, 4096 (2001).
- [2] W. Horton, *Rev. Mod. Phys.* **71**, 735 (1999).
- [3] Z. Gao, H. Sanuki, K. Itoh, and J. Q. Dong, *Phys. Plasmas* **10**, 2831 (2003).
- [4] B. Labit and M. Ottaviani, *J. Plasma Phys.* **73**, 199 (2007).
- [5] H. Y. Yun, F. M. Levinton, R. E. Bell, J. C. Hosea, S. M. Kaye, B. P. LeBlanc, E. Mazzucato, J. L. Peterson, D. R. Smith, J. Candy, R. E. Waltz, C. W. Domier, N. C. Luhmann, Jr., W. Lee, and H. K. Park, *Phys. Plasmas* **16**, 056120 (2009).
- [6] J. W. Connor and H. R. Wilson, *Plasma Phys. Control. Fusion* **36**, 719 (1994).
- [7] P. N. Guzdar, C. S. Liu, J. Q. Dong, and Y. C. Lee, *Phys. Rev. Lett.* **57**, 2812 (1986).
- [8] W. Horton, B. G. Hong, and W. M. Tang, *Phys. Fluids* **31**, 2971 (1988).
- [9] J. Q. Dong and W. Horton, *Phys. Fluids B* **5**, 1581 (1993).
- [10] M. A. Beer and G. W. Hammett, *Phys. Plasmas* **3**, 4046 (1996).
- [11] W. Dorland, F. Jenko, M. Kotschenreuther, and B. N. Rogers, *Phys. Rev. Lett.* **85**, 5579 (2000).
- [12] W. W. Lee and R. A. Santoro, *Phys. Plasmas* **4**, 169 (1997).
- [13] S. -I. Itoh and K. Itoh, *Phys. Rev. Lett.* **60**, 2276 (1988).
- [14] K. Itoh, S.-I. Itoh, M. Yagi, and A. Fukuyama, *Phys. Plasmas* **5**, 4121 (1998).
- [15] B. N. Rogers, W. Dorland, and M. Kotschenreuther, *Phys. Rev. Lett.* **85**, 5336 (2000).
- [16] A. Hirose, *Phys. Plasmas* **10**, 4561 (2003).
- [17] C. Holland and P. H. Diamond, *Phys. Plasmas* **11**, 1043 (2004).
- [18] Y. Idomura, S. Tokuda, and M. Wakatani, *Phys. Plasma* **6**, 4658 (1999).
- [19] J. Li and Y. Kishimoto, *Phys. Plasmas* **11**, 1493 (2004).
- [20] F. Ryter, Y. Camenen, J. C. DeBoo, F. Imbeaux, P. Mantica, G. Regnoli, C. Sozzi, U. Stroth, ASDEX Upgrade, DIII-D, FTU, JET-EFDA contributors, TCV, Tore Supra and W7-AS Teams, *Plasma Phys. Control. Fusion* **48**, B453 (2006).
- [21] E. Asp, J. -H. Kim, W. Horton, L. Porte, S. Alberti, A. Karpushov, Y. Martin, O. Sauter, G. Turri, and the TCV TEAM, *Phys. Plasmas* **15**, 082317 (2008).
- [22] E. Mazzucato, D. R. Smith, R. E. Bell, S. M. Kaye, J. C. Hosea, B. P. Leblanc, J. R. Wilson, P. M. Ryan, C. W. Domier, N. C. Luhmann, Jr., H. Yuh, W. Lee, and H. Park, *Nucl. Fusion* **49**, 055001 (2009).
- [23] G. T. Hoang, W. Horton, C. Bourdelle, B. Hu, X. Garbet, and M. Ottaviani, *Phys. Plasmas* **10**, 405 (2003).
- [24] F. Porcelli, E. Rossi, G. Cima, and A. Wootton, *Phys. Rev. Lett.* **82**, 1458 (1999).
- [25] M. M. Rahman, S. Tamura, S. Yanagi, T. Kaneko, and R. Hatakeyama, *Proceedings of International Interdisciplinary-Symposium on Gaseous and Liquid Plasma*, 97 (2008).